Design of a measurement cell for low-frequency dielectric spectroscopy of biological cell suspensions

AUTHOR(S):

Asami, Koji

CITATION:

Asami, Koji. Design of a measurement cell for low-frequency dielectric spectroscopy of biological cell suspensions. Measurement Science and Technology 2011, 22(8): 85801.

ISSUE DATE:

2011-08

URL:

http://hdl.handle.net/2433/145990

Design of a measurement cell for low-frequency dielectric spectroscopy of biological cell suspensions

Koji Asami
Institute for Chemical Research, Kyoto University, Uji, Kyoto 611-0011, Japan

E-mail: asami@e.kuicr.kyoto-u.ac.jp

Abstract

Dielectric spectroscopy of biological cell suspensions has a serious problem at low frequencies, where electrode polarization (EP) effects mostly mask their dielectric spectra. This paper describes a new type of measurement cell capable of extending the available low-frequency region by shifting the EP effects towards low frequencies. Its effectiveness was evaluated by computer simulation and experimental measurement on suspensions of erythrocytes and ghosts (hypotonically lysed erythrocytes). The results showed that the available low-frequency region was extended about ten times as compared with a corresponding conventional measurement cell, and that the low-frequency dispersion (so-called α-dispersion) of ghost suspensions was definitely observed.

Keywords: dielectric spectroscopy, biological cells, electrode polarization, erythrocytes, low-frequency dielectric dispersion

Subject classification number (PACS): 77.22.Gm, 83.80.Lz, 87.10.Kn, 87.15.Pc
Submitted to Measurement Science and Technology

1. Introduction

Dielectric spectra of biological cell suspensions show α- and β-dispersion in the radio-frequency range [1]. The β-dispersion is usually found above 10 kHz, being due to interfacial polarization or the Maxwell-Wagner effect. It is well understood and has been extensively and intensively studied [1-5]. In contrast to the β-dispersion, the α-dispersion that appears at the low-frequency (LF) side of the β-dispersion has difficulty in measurement, because it is mostly masked by the electrode polarization (EP) effect, which is due to an electric double layer at the interface between an electrode and an aqueous solution of electrolytes [6, 7]. A number of methods have been proposed to reduce and correct the EP effect [8-12]. Nevertheless, there has been no established method, and it is still difficult to get reliable data on the α-dispersion. In this study, a new measurement cell has been designed to extend the available low-frequency region by shifting the EP effect towards low frequencies.

2. Strategy to reduce the EP effect

A parallel-plate capacitor type of measurement cell (figure 1(*a*)) is commonly used for dielectric spectroscopy in the radio-frequency range. If the measurement cell is filled with an aqueous solution of electrolytes, the EP effect appears at low frequencies, say below 10 kHz, resulting from the impedance of the electrode interface. It is known that the electrode impedance Z_{el} has a constant phase angle element, i.e. $Z_{el} \propto (j\omega)^{-\alpha}$ with $0 \le \alpha \le 1$, $\omega = 2\pi f$, f frequency and $j = \sqrt{-1}$ [12]. If we adopt $\alpha = 1$ as a first approximation, Z_{el} has only a capacitance element, i.e. $Z_{el} = (j\omega C_{el})^{-1}$ with the electrode capacitance C_{el}. For the sake of simplicity, neglecting the capacitance of the solution, the electrode-solution system is simply represented by a series combination of C_{el} and the resistance R_s of the solution (figure 1(*b*)). The time constant of the electric circuit becomes $C_{el}R_s$, and the characteristic frequency of the EP effect is $1/(2\pi C_{el}R_s)$. Hence, we can shift the EP effect to the LF side by increasing C_{el} and/or R_s to extend the available low-frequency region. For increasing C_{el}, we often use Pt-black electrodes, whose effective surface area is increased by plating fine Pt-particles. A strategy to increase R_s independently of C_{el} is to increase the electrode distance besides reducing the sample conductivity. However, this is not so effective because the increased electrode distance reduces the measurement sensitivity and requires a large sample volume. Here, I propose an hourglass-shaped measurement cell (termed an H-cell) that has a neck in the middle between the electrodes (figure 1(*c*)). The neck part is the sample cavity for a cell suspension, being connected to the compartments filled with the suspending medium. The sample cavity and the neighboring compartments are separated by membranes that are freely permeable to ions but not to cells. The advantages of this type of measurement cell are as follows. (i) The value of R_s can be increased largely by decreasing the neck radius. (ii) Since the electric current converges on the sample cavity, the sample volume is extremely reduced keeping enough measurement sensitivity. The reduction of the sample volume is important because a large amount of purified biological cells is not easily obtainable. To my knowledge this type of measurement cell has never been designed for dielectric spectroscopy although similar conductometric cells are used for small sample volumes. In the following sections, the effectiveness of the H-cell will be evaluated by computer simulation and experimental measurement.

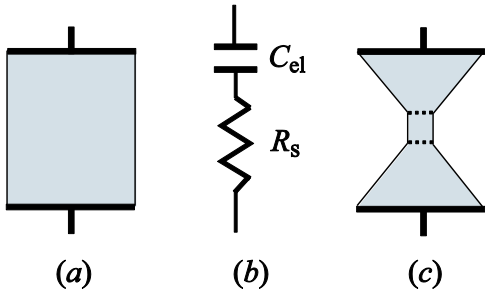

Figure 1. (*a*) A conventional measurement cell of parallel-plate electrodes, (*b*) its equivalent electric circuit model and (*c*) an hourglass-shaped measurement cell. The gray area is an aqueous solution of electrolytes or a sample cell suspension. The thick horizontal bars in (*a*) and (*c*) are electrodes. The broken lines in (*c*) indicate partitions that are freely permeable to ions but not to biological cells.

3. Evaluation of the cell design by computer simulation

3.1. Numerical calculation by the finite-element method

Figure 2 shows axisymmetric models H and C for the H-cell and the conventional measurement cell (termed the C-cell), respectively. The models consist of domains *a*, *b* and *c*, which have complex relative permittivities ε_a^*, ε_b^* and ε_c^*, respectively. Complex relative permittivity ε^* is defined as $\varepsilon^*=\varepsilon-j\kappa/(\omega\varepsilon_0)$, where ε is relative permittivity, κ is electric conductivity and ε_0 is the permittivity of vacuum. Domain *a* corresponds to an electrolyte solution, domain *b* is a sample, and domain *c* is an insulating spacer of $\varepsilon_c^*=3$. The distributions of electric potential ϕ in the models were numerically solved by a finite-element solver, COMSOL Multiphysics with an AC/DC Module (COMSOL AB, Sweden), in quasi-electrostatic and time-harmonics modes over a frequency range from 10 Hz to 100 MHz. The governing equation is the Laplace equation, i.e. $\nabla\cdot\left(\varepsilon^*\nabla\phi\right)=0$, and the boundary conditions are as follows. (i) At the symmetry axis and the insulated boundaries, $n\cdot J=0$ with the electric current density *J* and the unit vector *n* normal to the boundary. (ii) At the electrode boundaries, the specific capacitance C_p is placed to emulate the EP effect, with the boundary conditions being $n\cdot J=j\omega C_p\left(\phi-\phi_{ref}\right)$ with ϕ_{ref}=+1 and -1 V(RMS), respectively, for the top and bottom electrodes and C_p=88.5 mF/m^2, whose value is relevant to Pt-black electrodes. (iii) At the boundaries between neighboring domains, continuity of the electric current density hold, e.g. $n\cdot\left(J_a-J_b\right)=0$ for the boundary between domains *a* and *b*.

The solved electric potential distributions provide the electric current through the model by integrating the electric current density over the electrode boundary. Thus, the admittance of the model is calculated from the electric current and the applied voltage.

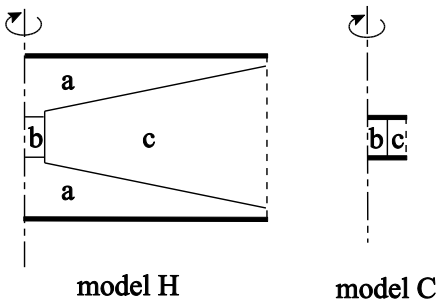

Figure 2. Axisymmetric models H and C for the H- and C-cells, respectively. Dash-dotted lines are the symmetric axes, broken lines are insulated boundaries, and thick solid lines are electrodes. Domain *a*, conical compartments; domain *b*, a cylindrical sample cavity; domain *c*, an insulating spacer. The radius of the circular electrodes is 15 mm, the cylindrical sample cavities of both models have the same geometry of a radius of 2 mm and a height of 4 mm.

3.2. Aqueous solutions of electrolytes

Here, we consider a simple case that domains *a* and *b* are the same aqueous solution, i.e. $\kappa_a=\kappa_b=0.1$ S/m and $\varepsilon_a=\varepsilon_b=80$. Figure 3 shows frequency dependence of the capacitance C and conductance G calculated for models H and C. The plots of log C against log f gave straight lines with negative slopes, which correspond to the EP effect. The EP effect of model H appeared at frequencies about ten times lower than that of model C. The EP effect was also seen in the G plots for model C below 100 Hz. At higher frequencies than 1 MHz, model H showed dielectric relaxation of a small intensity as shown in figure 4. The dielectric relaxation is due to the complex structure of model H where the electric field is non-uniform and is well represented by

$$C^* = C_h + \frac{\Delta C}{1+ j\, f/f_c} + \frac{G_l}{j\omega}, \qquad (1)$$

where C_h is the high-frequency limit of capacitance, ΔC is the relaxation intensity, f_c is the characteristic frequency and G_l is the low-frequency limit of conductance. The dielectric relaxation parameters C_h, ΔC, f_c and G_l were determined by fitting (1) to the dielectric relaxation, being listed in the row of $\kappa_b/\kappa_a=1$ in table 1.

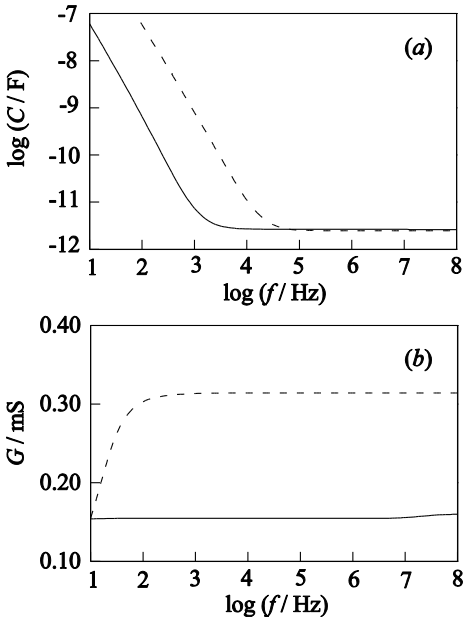

Figure 3. Frequency dependence of (*a*) capacitance *C* and (*b*) conductance *G* calculated for model H (solid lines) and model C (broken lines). The electric parameters of domains *a* and *b* are $\kappa_a=\kappa_b=0.1$ S/m and $\varepsilon_a=\varepsilon_b=80$.

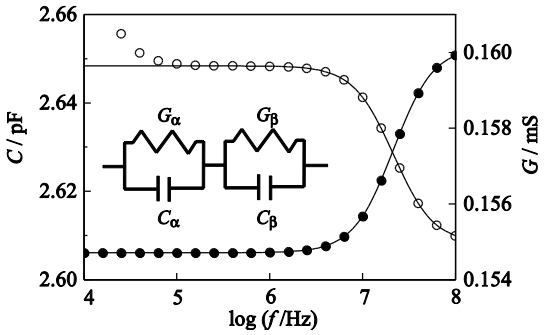

Figure 4. The HF dielectric relaxation of model H. Capacitance *C* (○) and conductance *G* (●) are plotted against frequency *f*. The data are the same as in figure 3. The solid lines are calculated from (1) with the dielectric relaxation parameters for $\kappa_b/\kappa_a=1$ in table 1. Inset: an equivalent electric circuit for model H. Subscripts α and β of *C* and *G* refer to circuits α and β, respectively.

To understand the HF dielectric relaxation of model H, further simulation was performed by varying the value of κ_b; the obtained dielectric relaxation parameters being summarized in table 1. As the κ_b/κ_a ratio deviates from unity, the value of ΔC increases, whereas the values C_h are almost independent of κ_b. The values of f_c and G_l increase with κ_b. That the dielectric relaxation is represented by (1) is interpreted in terms of the equivalent electric circuit model consisting of a serial combination of circuits α and β (figure 4, inset). The electric parameters of the electric circuit were determined from the dielectric relaxation parameters shown in table 1

by the method described previously [13, 14]. The results are summarized in table 2. The conductance G_β of circuit β is proportional to κ_b, suggesting that circuit β corresponds mainly to a region including domain *b*. However, the electric parameters of circuit α are also influenced by κ_b. It is therefore difficult to simply assign circuits α and β to domains *a* and *b*.

Table 1. Dielectric relaxation parameters of the high-frequency relaxation for varied κ_b/κ_a ratios

κ_b/κ_a	κ_b (S m^{-1})	C_h (pF)	ΔC (pF)	f_c (MHz)	G_l (mS)
5	0.5	2.62	0.474	59.6	0.255
1	0.1	2.61	0.0402	21.6	0.155
0.5	0.05	2.61	0.195	17.2	0.104
0.1	0.01	2.61	0.89	12.1	0.0285
0.05	0.005	2.61	1.07	11.5	0.0149

κ_a=0.1 S/m, $\varepsilon_a=\varepsilon_b$=80

Table 2. Equivalent electric circuit analysis of the data shown in table 1.

κ_b/κ_a	C_α (pF)	G_α (mS)	C_β (pF)	G_β (mS)
5	11.6	5.33	3.38	0.268
1	58.4	8.14	2.73	0.158
0.5	18.2	2.18	3.04	0.109
0.1	8.76	0.919	3.72	0.0294
0.05	8.27	0.858	3.81	0.0152

3.3. Dielectric cell constant and stray capacitance

The admittance obtained using a measurement cell is usually converted to the complex relative permittivity for subsequent theoretical analysis. For the conversion, we need the dielectric cell constant and the stray capacitance of the measurement cell, which are definitely determined using reference materials (e.g. air and water) for the C-cell. Those of the H-cell, however, are not uniquely determined and likely depend on the electric properties of the sample. To examine this problem, simulation was made by varying the relative permittivity ε_b and conductivity κ_b of domain *b* in model H in the absence of the EP effect. The capacitance was independent of frequency below 100 kHz, being directly proportional to ε_b at a fixed value of κ_b/κ_a (figure 5(*a*)). The proportional coefficient corresponding to the cell constant depends on the κ_b/κ_a ratio (figure 5(*b*)), whereas the intercept at ε_b=0, i.e., the stray capacitance, is almost constant. In conclusion, the cell constant is not determined uniquely but the capacitance is proportional to ε_b if the κ_b/κ_a ratio is unchanged.

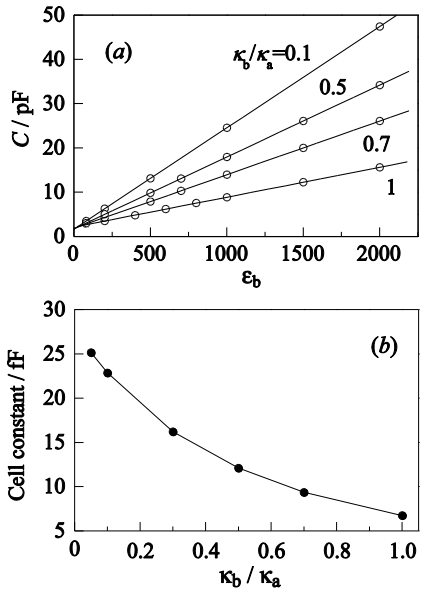

Figure 5. (*a*) The relationships between the capacitance *C* of model H and the relative permittivity ε_b of domain *b* at varied κ_b/κ_a ratios. The capacitance values at 40 kHz are used. Solid lines are linear regression lines, whose slopes provide the cell constant. (*b*) The cell constant is plotted against the κ_b/κ_a ratio.

3.4. Cell suspensions having α- and β-dispersion

Simulation was made for models H and C containing biological cell suspensions using the effective medium approximation [15], which simplifies numerical calculation by regarding a cell suspension as an effective medium. The complex relative permittivity ε_{susp}^* of a cell suspension was calculated by an analytical equation, being substituted for ε_b^* of domain *b* in the models. For the sake of simplicity, the spherical shell model was adopted, having a spherical cytoplasm (of the complex relative permittivity ε_{cp}^*) covered with a plasma membrane (of ε_{pm}^*). The ε_{susp}^* was calculated by the Pauly-Schwan theory [16]. The complex relative permittivity ε_{cell}^* of the cell is given by

$$\varepsilon_{cell}^* = \varepsilon_{pm}^* \frac{2\varepsilon_{pm}^* + \varepsilon_{cp}^* - 2v\left(\varepsilon_{pm}^* - \varepsilon_{cp}^*\right)}{2\varepsilon_{pm}^* + \varepsilon_{cp}^* + v\left(\varepsilon_{pm}^* - \varepsilon_{cp}^*\right)}, \tag{2}$$

where $v = \left(1 - d/R\right)^3$, *d* is the thickness of the plasma membrane and *R* is the radius of the cell.

When spherical cells of ε_{cell}^* are suspended in a medium of ε_m^* at volume fraction *P*, ε_{susp}^* is given by

$$\varepsilon_{susp}^* = \varepsilon_m^* \frac{2\varepsilon_m^* + \varepsilon_{cell}^* - 2P\left(\varepsilon_m^* - \varepsilon_{cell}^*\right)}{2\varepsilon_m^* + \varepsilon_{cell}^* + P\left(\varepsilon_m^* - \varepsilon_{cell}^*\right)}. \tag{3}$$

Since the conditions of $d/R \ll 1$ hold for biological cells, ε_{susp}^* shows one relaxation process

apart from the HF relaxation with a negligibly small intensity, and thus is approximately represented by

$$\varepsilon^*_{susp} = \varepsilon_h + \frac{\Delta\varepsilon_1}{1 + j\,f/f_{c1}} + \frac{\kappa_l}{j2\pi f\varepsilon_0}, \tag{4}$$

where ε_h is the HF limit of relative permittivity, $\Delta\varepsilon_1$ is the relaxation intensity, f_{c1} is the characteristic frequency and κ_l is the low-frequency limit of conductivity. The dielectric relaxation parameters ε_h, $\Delta\varepsilon_1$, f_{c1} and κ_l were calculated from the electric and geometrical parameters of the cells. In this simulation, the values used for the parameters in (2) and (3) were ε_m=80, κ_m=0.05 S/m, ε_{cp}=80, κ_{cp}=0.05 S/m, ε_{pm}=5, κ_{pm}=0, R=2.5 μm, d=5 nm and P=0.2. The resulting dielectric relaxation parameters in (4) became ε_h=79.5, $\Delta\varepsilon_1$=907, f_{c1}=258 kHz and κ_l=0.0364 S/m.

For a cell suspension showing the α- and β-dispersion, ε_{susp}^* is approximately represented by

$$\varepsilon^*_{susp} = \varepsilon_h + \frac{\Delta\varepsilon_1}{1 + j\,f/f_{c1}} + \frac{\Delta\varepsilon_2}{1 + j\,f/f_{c2}} + \frac{\kappa_l}{j2\pi f\varepsilon_0}, \tag{5}$$

where subscripts 1 and 2 refer to the β- and α-dispersion, respectively. With reference to the dielectric dispersion of erythrocyte ghosts [17], the relations of $\Delta\varepsilon_1=\Delta\varepsilon_2$ and $f_{c2}=f_{c1}/100$ were assumed, and the values used for the parameters in (5) were ε_h=79.5, $\Delta\varepsilon_1$=907, f_{c1}=258 kHz, $\Delta\varepsilon_2$=907, f_{c2}=2.58 kHz and κ_l=0.0364 S/m.

Substituting ε_{susp}^* for ε_b^* in models H and C, numerical simulation was carried out with and without the EP effect, and the resulting capacitance and conductance spectra are shown in figure 6. The EP effect of model H appeared at frequencies about ten times lower than that of model C, and thereby enabled us to see the α-dispersion clearly. This suggested that the H-cell is quite effective for investigating the α-dispersion. The spectra were analyzed using the following equation to determine the parameters of dielectric relaxation:

$$C^* = C_h + \frac{\Delta C_1}{1 + (j\,f/f_{c1})^{\beta_1}} + \frac{\Delta C_2}{1 + (j\,f/f_{c2})^{\beta_2}} + \frac{G_l}{j2\pi f} + Af^{-m}, \tag{6}$$

where subscripts 1 and 2 refer to the HF and the LF relaxation terms, Af^{-m} is the electrode polarization term of constants A and m. The relaxation parameters were obtained by fitting (6) to the dielectric spectra of figure 6, being listed in table 3. Since the EP effect mostly covered the LF dispersion with the C-cell, its parameters were not obtainable. In the absence of the EP effect, the $\Delta C_2/\Delta C_1$ ratio of model H was the same as that of model C, suggesting that the dielectric cell constant of model H can be obtained from that of model C and the relative value of ΔC_1 of the H-cell to the C-cell. The values of f_{c1} were somewhat different between the two models in contrast to f_{c2}, which means that the HF relaxation is likely distorted with model H. The EP effect caused some errors in estimation of ΔC_2 and f_{c2} for model H because of insufficient correction for the EP effect.

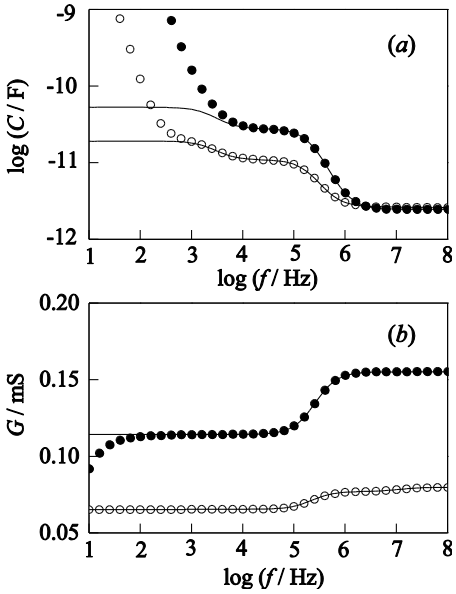

Figure 6. Frequency dependence of (*a*) capacitance *C* and (*b*) conductance *G* of models H and C containing a cell suspension showing α- and β-dispersion. Open and solid circles are data points for the H- and C-cells, respectively, in the presence of the EP effect, and solid lines in the absence of the EP effect.

Table 3. Relaxation parameters of the spectra shown in figure 6.

Models	EP	C_h (pF)	ΔC_1 (pF)	f_{c1} (kHz)	ΔC_2 (pF)	f_{c2} (kHz)	G_l (mS)
H	–	2.62	8.26	225	8.28	2.58	0.0653
C	–	2.46	25.2	258	25.2	2.58	0.114
H	+	2.62	8.27	226	7.40	2.94	0.0653
C	+	2.46	25.1	259	---	---	0.114

β_1=0.99-1.00, β_2=0.99-1.00

The H-cell has a great advantage for studying the LF dispersion, but includes some drawbacks: the HF spectra are likely distorted, and the dielectric cell constant is not simply determined. The drawbacks are overcome in the following way. (i) By measuring the same cell suspension using the H- and C-cells. (ii) By analyzing the capacitance spectra to determine the dielectric relaxation parameters: the HF limit C_{Hh} and the relaxation intensity ΔC_{H1} of the HF relaxation for the H-cell, and the high-frequency limit C_{Ch} and the relaxation intensity ΔC_{C1} of the HF relaxation for the C-cell. (iii) By calculating the relative permittivity $\varepsilon(f)$ from the capacitance data $C(f)$ of the H-cell as:

$$\varepsilon(f)=\frac{(C(f)-C_{Hh})(\Delta C_{C1}/\Delta C_{H1})+C_{Ch}-C_s}{C_0} \qquad (7)$$

where C_0 and C_s are respectively the dielectric cell constant and the stray capacitance of the C-cell. (iv) By replacing the HF data, say above 50 kHz, with those of the C-cell to remove uncertainty with the H-cell. This procedure was applied to the data in figure 6, providing dielectric spectra as shown in figure 7. Apart from the EP effect, the spectra are in a good agreement with the spectrum of ε_{susp}^* given in the simulation.

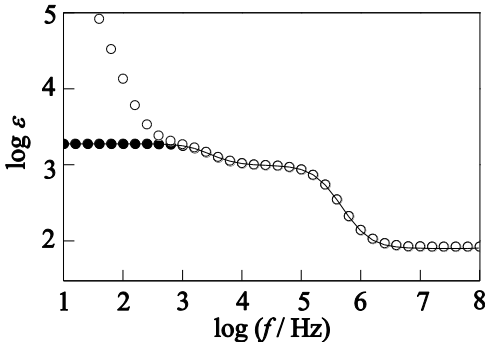

Figure 7. The relative permittivity spectra reproduced from the data (figure 6) without (●) and with (○) EP effect. The solid line is the true spectrum.

4. Experimental verification

4.1. Dielectric measurement

Figure 8 shows an H-cell made of polycarbonate, where a cylindrical sample cavity and two conical compartments are separated with cellulose membranes for dialysis (Eidia, Japan). A cell suspension was put into the sample cavity, and the conical compartments were filled with the suspending medium. The dialysis membrane is suitable for the partition because it is a quite small permeability barrier to small ions and therefore is nearly transparent electrically. The insertion of the dialysis membrane caused no discernible change in capacitance but only a 10 % reduction in conductance. The C-cell used was a parallel plate capacitor of a cylindrical sample cavity whose geometry was similar to that of the H-cell.

Dielectric measurement was carried out over a frequency range of 10 Hz to 10 MHz using a 4192A Impedance Analyzer (Agilent Technologies, USA). The H- and C-cells were fixed with a 16092A Spring Clip Fixture (Agilent Technologies, USA).

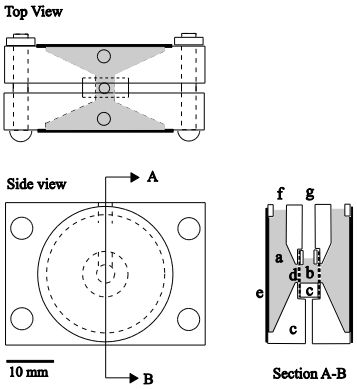

Figure 8. Diagram of the H-cell. (a) Compartment for medium, (b) sample cavity, (c) spacer of polycarbonate, (d) dialysis membrane, (e) Pt-black electrode, (f) medium inlet and (g) sample inlet.

4.2. Suspensions of erythrocytes and ghosts

The performance of the H-cell was evaluated using suspensions of horse erythrocytes and ghosts. Erythrocytes were prepared from preserved horse blood purchased from Nippon Biotest Lab. (Japan). The blood was centrifuged at 500 × g for 5 min to remove the plasma and the buffy coat, and the collected erythrocytes were washed twice with Dulbecco's phosphate buffered saline (PBS). The H-cell whose sample cavity and connecting compartments were respectively filled with the erythrocyte suspension and the suspending medium (PBS) was subjected to dielectric measurement. The same erythrocyte suspension was also measured using the C-cell. The results are shown in figure 9. Increases in *C* due to the EP effect were found at low frequencies below 10 kHz for the H-cell and 100 kHz for the C-cell. The available low-frequency region was definitely extended about ten times . The dielectric spectrum above 100 kHz is β-dispersion due to interfacial polarization, which is slightly distorted with the H-cell.

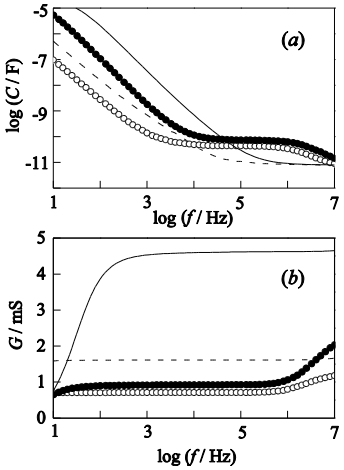

Figure 9. Frequency dependence of (*a*) capacitance *C* and (*b*) conductance *G* of an erythrocyte suspension measured using the H-cell (○) and the C-cell (●). Solid and broken lines are spectra of the medium (PBS) measured with the C- and H-cells, respectively. The medium conductivity is 1.29 S/m and temperature is 17ºC

Horse erythrocyte ghosts were prepared by hypotonic hemolysis as described in a previous paper [18]. Erythrocytes were washed with a 5 mM sodium phosphate buffer (pH 8) (NaP8) containing 0.15 M NaCl and then one part of the erythrocyte suspension was hemolysed by mixing with ten parts of a medium containing 5 mM NaP8 and 0.01 mM $MgSO_4$. The lysed erythrocytes were collected by centrifugation at 8,000 × g for 15 min and washed with a 5 mM sodium phosphate buffer (pH 7.2) (NaP7.2) containing 0.1 mM EDTA. Finally, white ghosts were obtained, which were resuspended in 5 mM NaP7.2 containing 10 mM NaCl and 0.1 mM EDTA. All operations in the ghost preparation were performed at 0-4ºC. Dielectric measurement was made at 15ºC. Figure 10 shows the dielectric spectra measured with the H- and C-cells. A large portion of the α-dispersion is clearly seen with the H-cell, whereas it is mostly covered with the EP effect for the C-cell.

Following the procedure described in section 3.4, the spectra of relative permittivity were obtained from the data in figures 9 and 10, and is shown in figure 11. The suspension of intact erythrocytes in PBS does not show any LF dispersion down to 10 kHz. The α-dispersion of ghost suspensions, which has never been traced since Schwan and Carstensen first reported it [17], has been evidently confirmed in this study using the H-cell. An investigation on the α-dispersion of ghost suspensions is undertaken and the results will be reported elsewhere.

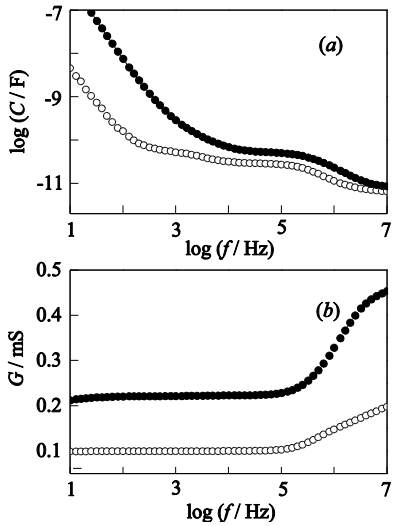

Figure 10. Frequency dependence of (*a*) capacitance *C* and (*b*) conductance *G* of a ghost suspension measured using the H-cell (○) and C-cell (●). Suspending medium is 5 mM NaP7.2 containing 10 mM NaCl and its conductivity is 0.143 S/m. Temperature is 15ºC

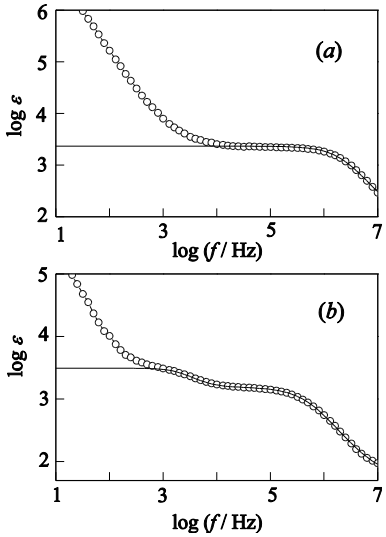

Figure 11. The relative permittivity spectra of (*a*) erythrocyte and (*b*) ghost suspensions, obtained from the data in figures 9 and 10. The open circles are data points and solid lines are the spectra corrected for the EP effect.

5. Concluding remarks

The effectiveness of the H-cell has been evaluated by computer simulation and experimental measurement. Computer simulation is useful for designing a measurement cell. Before making a prototype, we can check the effectiveness and drawbacks of the design. The experimental measurement demonstrated that the H-cell reduced the EP effect to extend the available low-frequency region about ten times compared with the conventional cell of a parallel-plate capacitor type. The H-cell allows accurate measurement of the α-dispersion of biological cell suspensions, thereby improving our understanding of its origin.

Particles with charged surfaces and polyelectrolytes in water show LF dielectric dispersion due to counterion polarization. The H-cell would be also applicable to suspensions of the particles and solutions of the polymers, providing reliable data on the LF dielectric dispersion.

Acknowledgment

This work was supported by a Grant-in-Aid for Scientific Research from the Japan Society for Promotion of Science.

References

[1] Schwan H P 1957 Electrical properties of tissue and cell suspensions *Advances in Biological and Medical Physics* (vol 5) ed J H Lawrence and C A Tobias (New York: Academic Press) pp 147-209

[2] Foster K R and Schwan H P 1996 Dielectric properties of tissues *Handbook of Biological Effects of Electromagnetic Fields* (2nd ed) ed C Polk and E Postow (Boca Raton: CRC Press) pp 25-102

[3] Pethig R and D B Kell 1987 The passive electrical properties of biological systems: their significance in physiology, biophysics and biotechnology *Phys. Med. Biol.* **32** 933-970

[4] Gimsa J and Wachner D 1998 A unified resistor-capacitor model for impedance, dielectrophoresis, electrorotation, and induced transmembrane potential *Biophys. J.* **75** 1107-1116

[5] Asami K 2002 Characterization of heterogeneous systems by dielectric spectroscopy *Prog. Polym. Sci.* **27** 1617-59

[6] Schwan H P 1963 Determination of biological impedances. *Physical Techniques in Biological Research* (vol 6) ed W Nastuk (New York: Academic Press) pp 323-407

[7] Schwan H P and Onaral B 1985 Linear and nonlinear properties of platinum electrode polarization III: equivalence of frequency- and time-domain behavior Med. Biol. Eng. Comput. **23** 28-32

[8] Schwan H P and Ferris C D 1968 Four-terminal null techniques for impedance measurements with high resolution *Rev. Sci. Instrum.* **39** 481-5

[9] Harris C M, Todd R W, Bungard S J, Lovitt R W, Morris G and Kell D B 1987 Dielectric permittivity of microbial suspensions at radio frequencies: a novel method for the real-time estimation of microbial biomass *Enzyme Microb. Technol.* **9** 181-6

[10] Asami K, Gheorghiu E and Yonezawa T 1999 Real-time monitoring of yeast cell division by dielectric spectroscopy *Biophys. J.* **76** 3345-8

[11] Raicu V, Saibara T and Irimajiri A 1998 Dielectric properties of rat liver in vivo: a non invasive approach using an open-ended coaxial probe at audio/radio frequencies *Bioelectrochem. Bioenerg.* **47** 325-32

[12] Bordi F, Cametti C and Gili T 2001 Reduction of the contribution of electrode polarization effects in the radiowave dielectric measurements of highly conductive biological cell suspensions *Bioelectrochem.* **54** 53-61

[13] Zhang H, Hanai T and Koizmi N 1983 Dielectric analysis of interfacial polarization in bilamellar structure as applied to underwater polystyrene films *Bull. Inst. Chem. Res., Kyoto Univ* **61** 265-281

[14] Zhang H, Sekine K, Hanai T and Koizumi N 1983 Dielectric properties of underwater polystyrene films related to microcapsules *Membrane* **8** 249-254

[15] Asami K 2010 Effectiveness of “thin-layer” and “effective medium” approximations in numerical simulation of dielectric properties of biological cell suspensions *Jpn. J. Appl. Phys.* **49** 127001

[16] Pauly H and Schwan H P 1959 Über die Impedanz einer Suspension von Kugelförmigen Teilchen mit einer Schale *Z. Naturforsch.* **14b** 125-131

[17] Schwan H P and Carstensen E L 1957 Dielectric properties of the membrane of lysed erythrocytes *Science* **125** 985-6

[18] Lieber M R and Steck T L 1982 A description of the holes in human erythrocyte membrane ghosts *J. Biol. Chem.* **257** 11651-11659